Downloaded from SAE International by Georgia Institute of Technology, Sunday, April 06, 2025

2025-01-8811 Published 01 Apr 2025

Stability Control for Distributed Drive Electric Vehicles Using Particle Filter and Fuzzy Integral Sliding Mode Control

Xiaolong Li and Hongyu Zheng Jilin University

Chuyo Kaku Jiangsu Chaoli Electric Co., Ltd.

Citation: Li, X., Zheng, H., and Kaku, C., "Stability Control for Distributed Drive Electric Vehicles Using Particle Filter and Fuzzy Integral Sliding Mode Control," SAE Technical Paper 2025-01-8811, 2025, doi:10.4271/2025-01-8811.

Received: 08 Oct 2024 Revised: 16 Jan 2025 Accepted: 18 Jan 2025

Abstract

The Distributed Drive Electric Vehicles (DDEVs) offer advantages such as independently controllable driving and braking forces at each wheel, rapid response, and precise control. These features enable effective electronic stability control (ESC) by appropriately distributing torque across each wheel. However, traditional ESC systems typically employ single-wheel hydraulic differential braking, failing to fully utilize the independent torque control capabilities of DDEVs. This study proposes a hierarchical control strategy for distributed driving and braking ESC based on particle filter (PF) and fuzzy integral sliding mode control (FISMC). First, the vehicle state estimation layer uses a three-degree-of-freedom vehicle model and the PF to estimate sideslip angle and vehicle speed. Next, the target torque decision layer includes a target speed tracking controller and a yaw moment decision controller. The yaw moment decision controller uses the FISMC to determine additional yaw moment by comparing the estimated yaw rate and sideslip angle with their ideal values, while dynamically adjusting the sliding mode surface parameters based on vehicle state and driving conditions. Finally, the dynamic torque distribution layer allocates the driving and regenerative braking torques to each wheel according to changes in vertical tire load. A co-simulation platform using MATLAB/Simulink and CarSim is established to validate the proposed control strategy under double lane change and J-turn maneuvers, comparing it with traditional ESC. The results show that the proposed ESC achieves high accuracy in estimating vehicle state and effectively adapts to varying driving conditions while maintaining stable vehicle speed, thereby enhancing driving stability.

Introduction

The development of electric vehicles presents an effective solution to fossil fuel shortages and vehicle exhaust pollution. Advancements in motor technology have given rise to the Distributed Drive Electric Vehicles (DDEVs), which feature independent wheel drive. Unlike traditional vehicles that rely on internal combustion engines and hydraulic braking systems, DDEVs utilize individual motors for each wheel to provide driving and braking torque. These motors offer rapid response, precise control, and easily accessible speed and torque. This configuration significantly enhances the active safety of the vehicle.

Electronic Stability Control (ESC) is a critical technology for ensuring vehicle active safety. Each motor of DDEVs can be independently controlled and can swiftly switch between driving and braking states, enabling continuous and efficient stability control. However, traditional ESC systems primarily rely on single-wheel hydraulic differential braking, which fails to fully utilize the independent drive and braking capabilities of DDEVs. Additionally, the activation of traditional ESC significantly reduces vehicle speed and causes noticeable intervention, adversely affecting driving comfort [1]. Therefore, traditional stability control strategies are inadequate for DDEVs and require redesign and further research.

The sideslip angle is a critical control variable in vehicle stability control. Given the high cost associated with directly measuring the sideslip angle using sensors, indirect estimation methods based on multi-information fusion observers are predominantly utilized. Common observers include Kalman filters, Luenberger observers [2], sliding mode observers, and robust observers [3]. Mengjie Tian et al. developed a sideslip angle estimator based on a nonlinear two-degree-of-freedom vehicle dynamics model and the Extended Kalman Filter (EKF)

Downloaded from SAE International by Georgia Institute of Technology, Sunday, April 06, 2025

method, demonstrating the estimator's effectiveness under double lane change maneuver [4]. Wang Hongbo et al. established a fuzzy second-order sliding mode observer to enhance the accuracy and real-time performance of sideslip angle estimation. They corrected the observed sideslip angle using integrated estimates from sensor signals, achieving reliable estimation [5]. Pan Wang et al. focused on distributed drive electric vehicles and utilized the Unscented Kalman Filter (UKF) method to accurately estimate the sideslip angle [6]. However, in the presence of strong nonlinearity and non-Gaussian characteristics in vehicle systems, the accuracy of state parameter estimation using Kalman filter and its derived algorithms is limited [7]. If the estimation accuracy of the sideslip angle does not satisfy the control requirements of ESC system, it may result in vehicle instability and pose significant safety risks.

ESC system stabilizes a vehicle's lateral motion by applying driving or braking forces to the inner and outer wheels, thereby generating additional yaw moments that enhance handling stability. The algorithms for determining these additional yaw moments include PID control [8], fuzzy control [9], sliding mode control, and Model Predictive Control [10]. Mats Jonasson et al. employed the vehicle's yaw rate and sideslip angle as control variables, implementing a PID for electric vehicle ESC [11]. While this algorithm is straightforward and reliable, simulation results under varying conditions demonstrate that PID has limited adaptability to nonlinear systems and parameter variations. Yitong Song et al. proposed a hierarchical control strategy for the nonlinear characteristics of ESC system. In the upper layer, a sliding mode control algorithm is employed to calculate the additional yaw moment, while in the lower layer, a weighted least squares method is used to optimize torque distribution. Simulation results indicate that the proposed control strategy enhances vehicle handling stability [12]. Chunyun Fu et al. focused on independently motor-driven electric vehicles and utilized a sliding mode control algorithm with a novel switching function to determine the additional yaw moment, aiming to track the ideal yaw rate and sideslip angle [13]. Given the complexity and variability of vehicle instability scenarios, it is essential to enhance the adaptability of torque decision algorithms under various driving conditions.

Based on the previous analysis, this study investigates a hierarchical control strategy for distributed driving and braking ESC based on PF and FISMC. First, the vehicle state estimation layer employs a three-degree-of-freedom (3DOF) model and the PF to estimate vehicle state. Subsequently, the target torque decision layer is comprised of a Proportional-Integral (PI) speed tracking controller and a yaw moment decision controller. The yaw moment decision controller leverages the FISMC to calculate additional yaw moment by comparing estimated and ideal values for yaw rate and sideslip angle, while dynamically adjusting the sliding mode surface based on vehicle state and driving conditions. Finally, the torque distribution layer allocates driving and braking torque to each wheel in response to variations in tire vertical load. Under double lane change and J-turn maneuvers, a co-simulation platform is established using MATLAB/Simulink and CarSim to evaluate the effectiveness of the proposed control strategy.

This paper is structured as follows: Section 2 introduces the distributed driving and braking ESC control framework. Section 3 develops vehicle dynamic models. Section 4 presents a hierarchical stability control strategy with vehicle state estimation, target torque decision, and dynamic torque distribution layers. Section 5 offers simulation validation, followed by a summary of the findings.

Framework of Stability Control

This section introduces a hierarchical control framework for distributed driving and braking ESC, utilizing PF and FISMC, as illustrated in Figure 1. The framework consists of three layers: vehicle state estimation, target torque decision, and dynamic torque distribution. In the vehicle state estimation layer, a 3DOF vehicle model and the PF algorithm are employed to estimate real-time vehicle states, such as the sideslip angle and longitudinal speed, to support subsequent stability control. The target torque decision layer comprises two controllers: a target speed tracking controller and a yaw moment decision controller. The target speed tracking controller uses the PI to determine the target driving torque. The yaw moment decision controller utilizes the estimated yaw rate and sideslip angle, comparing them with ideal values from a two-degree-of-freedom (2DOF) vehicle model. An integral sliding mode control is then applied to determine the additional yaw moment, with the sliding mode surface dynamically adjusted using fuzzy control to enhance adaptability across varying driving conditions. In the dynamic torque distribution layer, driving and regenerative braking torques are dynamically allocated based on changes in tire vertical load. Finally, the actual driving and braking torques for each wheel are generated and executed by the four in-wheel motors, completing the entire ESC control process.

FIGURE 1 Proposed framework for distributed driving and braking ESC.

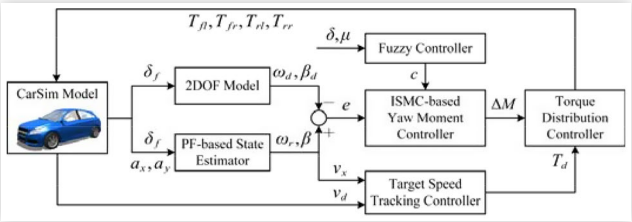

Downloaded from SAE International by Georgia Institute of Technology, Sunday, April 06, 2025

Vehicle Dynamic Model

To meet the requirements for vehicle state estimation and the design of stability control strategy, this section establishes 3DOF and 2DOF vehicle dynamic models.

Three-Degree-of-Freedom Model

A 3DOF model, incorporating longitudinal, lateral, and yaw motions as shown in Figure 2, is developed to estimate vehicle state such as the sideslip angle. The influence of the steering system is neglected, with the front wheel steering angle taken as the model input. Similarly, the effects of the suspension system are disregarded, assuming planar motion parallel to the ground. The dynamic equilibrium equations for the 3DOF model are presented in equations (1) through (3).

$$\begin{aligned} ma_x &= m\left(\dot{v}_x - \omega_r \cdot v_y\right) = \left(F_{xfl} + F_{xfr}\right)\cos\delta_f \\ &-\left(F_{yfl} + F_{yfr}\right)\sin\delta_f + F_{xrl} + F_{xrr} \end{aligned} \tag{1}$$

$$\begin{aligned} ma_y &= m\left(\dot{v}_y + \omega_r \cdot v_x\right) = \left(F_{xfl} + F_{xfr}\right)\sin\delta_f \\ &+\left(F_{yfl} + F_{yfr}\right)\cos\delta_f + F_{yrl} + F_{yrr} \end{aligned} \tag{2}$$

$$\begin{aligned} I_z\dot{\omega}_r &= \left[\left(F_{xfl} + F_{xfr}\right)\sin\delta_f + \left(F_{yfl} + F_{yfr}\right)\cos\delta_f\right]a \\ &+\left[\left(F_{xfr} - F_{xfl}\right)\cos\delta_f + \left(F_{yfl} - F_{yfr}\right)\sin\delta_f\right]\frac{B}{2} \\ &+\left(F_{xrr} - F_{xrl}\right)\frac{B}{2} - \left(F_{yrl} + F_{yrr}\right)b \end{aligned} \tag{3}$$

where m is the vehicle mass, v_x and v_y are the longitudinal and lateral vehicle speeds, respectively. a_x and a_y are the longitudinal and lateral accelerations, respectively. ω_r is the yaw rate, δ_f are the steering angle of the front wheels. F_{xij} and F_{yij} are the longitudinal and lateral tire forces, respectively, with subscripts *fl*, *fr*, *rl* and *rr* denoting the left front, right front, left rear, and right rear wheels, respectively. a is distance from center of mass to front axle and b is distance from center of mass to rear axle, B is tread, and I_z is yaw moment of inertia.

FIGURE 2 Three-degree-of-freedom vehicle model.

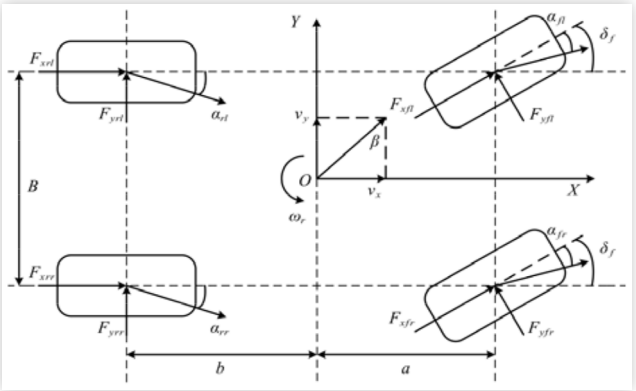

Assuming a linear relationship between the tire's lateral force and the sideslip angle, the lateral force can be expressed as:

$$F_{yij} = k_{ij}\alpha_{ij} \tag{4}$$

where k_{ij} is the tire cornering stiffness, α_{ij} is the sideslip angle. The approximate expressions for the sideslip angles of the tires on the front and rear axles are:

$$\begin{cases} \alpha_{fl} = \alpha_{fr} = \delta_f - \dfrac{v_y + a\omega_r}{v_x} \\ \alpha_{rl} = \alpha_{rr} = -\dfrac{v_y - b\omega_r}{v_x} \end{cases} \tag{5}$$

Two-Degree-of-Freedom Model

The 2DOF model is crucial for analyzing vehicle lateral stability. This model builds upon the 3DOF model, assuming constant forward speed and neglecting variations in tire lateral stiffness [14]. Consequently, the 2DOF model is established, with the differential equations of motion expressed as follows [15]:

$$\begin{cases} \dot{\beta} = \dfrac{k_f + k_r}{mv_x}\beta + \left(\dfrac{ak_f - bk_r}{mv_x^2} - 1\right)\omega_r - \dfrac{k_f}{mv_x}\delta_f \\ \dot{\omega}_r = \dfrac{ak_f - bk_r}{I_z}\beta + \dfrac{a^2k_f + b^2k_r}{I_z v_x}\omega_r - \dfrac{ak_f}{I_z}\delta_f \end{cases} \tag{6}$$

where β is the sideslip angle. When the vehicle is in a stable state, the yaw rate and sideslip angle remain constant, i.e., $\dot{\omega}_r = 0, \dot{\beta} = 0$. Substituting these conditions into equation (6) yields the ideal values for the yaw rate ω_{rd} and the ideal sideslip angleβ_d:

$$\begin{cases} \omega_{rd} = \dfrac{v_x / l}{1 + Kv_x^2}\delta_f \\ \beta_d = \dfrac{2b\left(a+b\right)k_f k_r - mv_x^2 ak_f}{2b\left(a+b\right)^2 k_f k_r - mv_x^2\left(ak_f - bk_r\right)}\delta_f \end{cases} \tag{7}$$

where l is the wheelbase. To effectively prevent vehicle sideslip and ensure adherence to the driver's desired trajectory, the ideal sideslip angle is defined as [16]: $\beta_d = 0$.

The lateral acceleration of the vehicle during steering is constrained by the road surface, thereby defining the upper limit of the yaw rate $|\omega_{r\max}|$ as follows:

$$\left|\omega_{r\max}\right| = \frac{\mu g}{v_x} \tag{8}$$

where μ is the road adhesion coefficient, g is the gravitational acceleration.

Based on the analysis above, the ideal yaw rate ω_{rd} and the ideal sideslip angle β_d are revised as follows:

$$\begin{cases} \omega_{rd} = \min\left\{\left|\dfrac{v_x / l}{1 + Kv_x^2}\delta_f\right|, \left|\omega_{r\max}\right|\right\} \cdot \mathrm{sgn}\left(\delta_f\right) \\ \beta_d = 0 \end{cases} \tag{9}$$

Downloaded from SAE International by Georgia Institute of Technology, Sunday, April 06, 2025

Methodology for Stability Control

This section utilizes the four-wheel independent controllability of DDEVs to investigate a hierarchical ESC strategy, comprising a vehicle state estimation layer, a target torque decision layer, and a dynamic torque distribution layer.

Vehicle State Estimation Layer

DDEVs are typical nonlinear systems that frequently encounter non-Gaussian noise during operation. Compared to Kalman filter, particle filter offers unique advantages in nonlinear and non-Gaussian systems [17]. Therefore, a particle filter algorithm is employed in this study to estimate vehicle states, such as the sideslip angle, thereby enhancing estimation accuracy.

From equations (1) to (3), the state and observation equations of the 3DOF vehicle model are obtained:

$$\begin{cases} \dot{\omega}_r = \dfrac{ak_f - bk_r}{I_z}\beta + \dfrac{a^2k_f + b^2k_r}{I_z v_x}\omega_r - \dfrac{ak_f}{I_z}\delta_f \\ \dot{\beta} = \dfrac{k_f + k_r}{mv_x}\beta + \left(\dfrac{ak_f - bk_r}{mv_x^2} - 1\right)\omega_r - \dfrac{k_f}{mv_x}\delta_f \\ \dot{v}_x = \omega_r \beta v_x + a_x \end{cases} \tag{10}$$

$$a_y = \frac{ak_f - bk_r}{mv_x}\omega_r + \frac{k_f + k_r}{m}\beta - \frac{k_f}{m}\delta_f \tag{11}$$

From equations (10) and (11), the state variables of the vehicle state estimation system are yaw rate, sideslip angle, and longitudinal speed, namely $x=[\omega_r, \beta, v_x]^T$; the input variables are the front wheel steering angle and longitudinal acceleration, namely $u=[\delta_f, a_x]^T$; and the observed variable is the lateral acceleration, namely $y=a_y$. Using the Euler method, the state and observation equations are discretized as follows:

$$\begin{cases} x_{k+1} = f\left(x_k, u_k\right) + w_k \\ y_k = h\left(x_k, u_k\right) + v_k \end{cases} \tag{12}$$

where, x_k represents the state variables, u_k represents the input variables, y_k represents the observation variables, w_k denotes the process noise with covariance Q, v_k denotes the observation noise with covariance R, w_k and v_k are uncorrelated.

The core concept of particle filter involves approximating the system's probability density distribution using a set of weighted particles, thus achieving state estimation [18]. The steps for estimating vehicle state using the particle filter algorithm are as follows:

Step 1: Initialization at time

Extract N particles $\left\{x_0^{(i)}\right\}_{i=1}^{N}$ from the prior distribution $p(x_0)$, and set each particle's initial weight to $w_0^{(i)} = 1/N$.

Step 2: For $k \geq 1$, repeatedly execute the following process:

(a) Importance sampling.

Since directly extracting particles from the posterior distribution $p(x_{k+1}|y_{k+1})$ is difficult, particles $\left\{\tilde{x}_{k+1}^i\right\}_{i=1}^{N}$ are drawn from a known and easily sampled reference distribution $q(x_{k+1}|y_{k+1})$.The weight of each particle w_{k+1}^i is calculated as follows:

$$w_{k+1}^i \propto w_k^i \frac{p\left(y_{k+1}|x_{k+1}^i\right)p\left(x_{k+1}^i|x_k^i\right)}{q\left(\tilde{x}_{k+1}^i|,\tilde{x}_k^i|,y_{k+1}\right)} \tag{13}$$

Normalize the particle weights to:

$$\tilde{w}_{k+1}^i = \frac{w_{k+1}^i}{\sum_{i=1}^{N} w_{k+1}^i} \tag{14}$$

(b) Resampling.

In practical applications of particle filtering, particle weights can degrade as the number of samples increases, leading to inefficient use of computational resources. To address this issue, resampling is necessary. This paper utilizes the residual resampling method, which resets each particle's weight to:

$$w_{k+1}^{(i)} = 1/N \tag{15}$$

(c) State variable output.

Following the aforementioned steps, the state variable estimates derived from the particle filter are obtained:

$$\hat{x}_{k+1} = \sum_{i=1}^{N} x_{k+1}^i w_{k+1}^i \tag{16}$$

Target Torque Decision Layer

Target Speed Tracking Controller The objective of target speed tracking is to ensure that the actual vehicle speed follows the desired target speed in real-time under both normal driving and stability control modes. The target speed tracking controller utilizes a PI control to determine the required drive torque based on the difference between the actual speed and the target speed, as given in equation (17). The target speed is set in CarSim software, and the actual speed is estimated by the state estimator. The principle for target speed tracking controller is illustrated in Figure 3.

$$T_d = K_p\left(v_d - v_x\right) + K_i \int \left(v_d - v_x\right) dt \tag{17}$$

where T_d denotes the total driving torque, v_d is the target speed, v_x is the estimated longitudinal speed, and K_p and K_i are the proportional and integral coefficients, respectively.

Downloaded from SAE International by Georgia Institute of Technology, Sunday, April 06, 2025

FIGURE 3 Schematic of the target speed tracking controller.

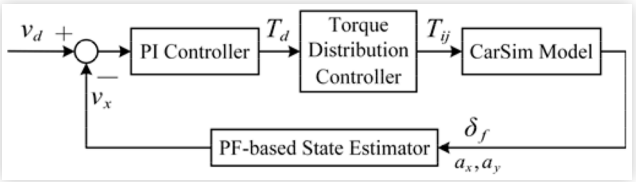

Yaw Moment Decision Controller Given the nonlinear characteristics of the ESC system, a sliding mode algorithm is employed to determine the additional yaw moment required to maintain vehicle stability. To enhance control accuracy while mitigating chattering, an integral sliding mode algorithm is utilized for vehicle lateral stability control [19].

The primary role of ESC is to maintain stability while ensuring the vehicle follows the driver's intended trajectory. Steering capability and stability depend on the yaw rate, while trajectory tracking is determined by the sideslip angle. To enhance stability control, both yaw rate and sideslip angle are used as control variables. Accordingly, the control error e n the integral sliding mode algorithm is defined as:

$$e = \omega_r - \omega_{rd} + \rho\left(\beta - \beta_d\right) \tag{18}$$

where ρ is the weighting factor.

To reduce the adverse effects of external disturbances, a sliding surface s with an integral term is designed, namely:

$$s = e + c\int e dt \tag{19}$$

where the integration coefficient c affects the convergence rate of the control deviation, with larger values leading to faster convergence.

In the two-degree-of-freedom vehicle model, the additional yaw moment ΔM necessary for maintaining lateral stability is introduced, resulting in the revised equation (6) as follows:

$$\begin{cases} \dot{\beta} = \dfrac{k_f + k_r}{mv_x}\beta + \left(\dfrac{ak_f - bk_r}{mv_x^2} - 1\right)\omega_r - \dfrac{k_f}{mv_x}\delta_f \\ \dot{\omega}_r = \dfrac{ak_f - bk_r}{I_z}\beta + \dfrac{a^2k_f + b^2k_r}{I_z v_x}\omega_r - \dfrac{ak_f}{I_z}\delta_f + \dfrac{\Delta M}{I_z} \end{cases} \tag{20}$$

Taking the derivative of equation (19) and substituting in equations (18) and (20):

$$\begin{aligned} \dot{s} &= \dot{e} + ce \\ &= \dot{\omega}_r - \dot{\omega}_{rd} + \rho\left(\dot{\beta} - \dot{\beta}_d\right) + c\left[\omega_r - \omega_{rd} + \rho\left(\beta - \beta_d\right)\right] \\ &= \frac{ak_f - bk_r}{I_z}\beta + \frac{a^2k_f + b^2k_r}{I_z v_x}\omega - \frac{ak_f}{I_z}\delta_f + \frac{\Delta M}{I_z} - \dot{\omega}_{rd} \\ &\quad + \rho\left[\frac{k_f + k_r}{mv_x}\beta + \left(\frac{ak_f - bk_r}{mv_x^2} - 1\right)\omega - \frac{k_f}{mv_x}\delta_f\right] - \rho\dot{\beta}_d \\ &\quad + c\left[\omega_r - \omega_{rd} + \rho\left(\beta - \beta_d\right)\right] \end{aligned} \tag{21}$$

To facilitate the transition of the system into the sliding mode and ensure stable operation, an exponential reaching law is adopted. Furthermore, to mitigate chattering, a saturation function is employed in place of the sign function, as follows:

$$\dot{s} = -\varepsilon sat\left(s\right) - ks \tag{22}$$

where ε and k represent the coefficients of the sliding reaching law, ks denotes the exponential term, and $sat(s)$ is the saturation function, as follows:

$$sat\left(s\right) = \begin{cases} 1, & s \geqslant \phi \\ s/\phi, & |s| < \phi \\ -1, & s \leqslant -\phi \end{cases} \tag{23}$$

where ϕ is the boundary layer thickness.

By combining equations (21) and (22), the additional yaw moment ΔM is given by:

$$\begin{aligned} \Delta M &= I_z\left[-\varepsilon sat\left(s\right) - ks\right] - \left(ak_f - bk_r\right)\beta - \frac{a^2k_f + b^2k_r}{v_x}\omega \\ &\quad + ak_f\delta_f + I_z\dot{\omega}_{rd} - I_z\rho\dot{\beta}_d - I_z c\left[\omega_r - \omega_{rd} + \rho\left(\beta - \beta_d\right)\right] \\ &\quad - I_z\rho\left[\frac{k_f + k_r}{mv_x}\beta + \left(\frac{ak_f - bk_r}{mv_x^2} - 1\right)\omega - \frac{k_f\delta_f}{mv_x}\right] \end{aligned} \tag{24}$$

To verify the stability of the system, a Lyapunov function is utilized as the stability criterion:

$$V = \frac{1}{2}s^2 \tag{25}$$

Differentiating equation (25) and substituting the relevant parameters, the following result is obtained:

$$\begin{aligned} \dot{V} &= s\dot{s} \\ &= s\left\{\dot{\omega}_r - \dot{\omega}_{rd} + \rho\left(\dot{\beta} - \dot{\beta}_d\right) + c\left[\omega_r - \omega_{rd} + \rho\left(\beta - \beta_d\right)\right]\right\} \\ &= -s\left(\varepsilon sat\left(s\right) + ks\right) = -\varepsilon\left|ssat\left(s\right)\right| - ks^2 \end{aligned} \tag{26}$$

since $\varepsilon > 0$, $k > 0$, it follows that $\dot{V} < 0$, indicating system stability.

To enhance the adaptability of the integral sliding mode controller under diverse driving conditions, a fuzzy controller is integrated to dynamically adjust the sliding mode surface in response to changes in vehicle state and driving scenarios. The inputs to the fuzzy controller include the road adhesion coefficient μ and the steering wheel angle δ, and output is the integral term coefficient c of the sliding mode surface. By monitoring variations in the steering wheel angle and road adhesion coefficient, the system dynamically adjusts the convergence rate of the control deviation, thereby optimizing vehicle stability.

The fuzzy domain for the steering wheel angle is defined as [0, 150] and is divided into seven levels. The fuzzy domain for the road adhesion coefficient is [0.2, 1], divided into five levels. The fuzzy domain for the integral term coefficient is [18, 30], also divided into seven levels. Triangular membership functions are employed due to

Downloaded from SAE International by Georgia Institute of Technology, Sunday, April 06, 2025

their computational efficiency, ensuring real-time performance in vehicle stability control. The membership function curves for input and output variables are illustrated in Figure 4. When the steering wheel angle is large and the road adhesion coefficient is low, the vehicle is prone to instability, requiring a rapid reduction in control error to converge the system to the sliding mode surface and maintain stability. Conversely, when the steering wheel angle is small and the road adhesion coefficient is high, effective suppression of chattering is necessary. Based on this analysis, fuzzy control rules for the integral term coefficient of the sliding mode surface are established, as presented in Table 1.

FIGURE 4 Membership function: (a) Steering wheel angle. (b) Road adhesion coefficient. (c) Integral term coefficient of the sliding mode surface.

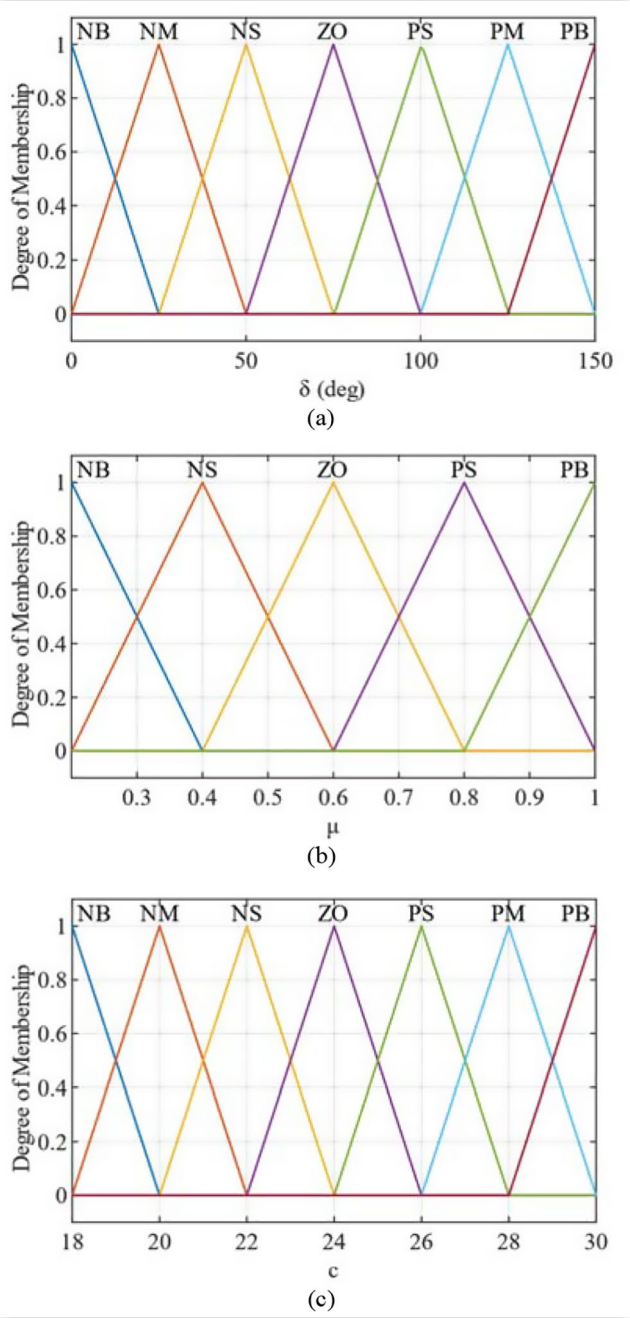

TABLE 1 Fuzzy rules for integral term coefficient of the sliding mode surface.

μ \ δ	NB	NM	NS	ZO	PS	PM	PB
NB	ZO	PS	PM	PM	PB	PB	PB
NS	NS	ZO	PS	PM	PM	PB	PB
ZO	NM	NS	ZO	PS	PM	PM	PB
PS	NB	NM	ZO	ZO	ZO	PM	PM
PB	NB	NM	NS	NS	NS	PS	PM

The design of the yaw moment decision controller based on FISMC has been completed. By incorporating the integral term, the proposed FISMC not only facilitates smooth switching on the sliding surface, alleviating the chattering phenomenon inherent in traditional SMC, but also enhances compensation capability by accumulating system deviations, thereby suppressing unknown disturbances more effectively. Moreover, unlike traditional PID controllers with fixed gains, the FISMC dynamically adjusts the sliding mode integral term coefficient in response to variations in road adhesion and vehicle state, through the fuzzy control mechanism. This dynamic adjustment enhances adaptability to varying driving conditions, significantly improves stability control performance.

Dynamic Torque Distribution Layer

During vehicle acceleration and deceleration, the presence of longitudinal acceleration results in varying vertical loads on the front and rear wheels. When the road adhesion coefficient is constant, the maximum adhesion force provided by the ground is determined by the vertical load on the tires [20]. Therefore, to maximize road adhesion and enhance control effectiveness, the driving/braking torque for each wheel motor is dynamically allocated based on changes in vertical load to meet the requirements for lateral stability control and target speed tracking.

The four wheel torques must meet the requirements for tracking target speed and generating additional yaw moment, as follows:

$$\begin{cases} T_d = T_{fl} + T_{fr} + T_{rl} + T_{rr} \\ \Delta M = \dfrac{B}{2r}\left(T_{fr} - T_{fl}\right) + \dfrac{B}{2r}\left(T_{rr} - T_{rl}\right) \end{cases} \tag{27}$$

where T_{fl}, T_{fr}, T_{rl}, and T_{rr} represent the motor torques for the left front wheel, right front wheel, left rear wheel, and right rear wheel, respectively, and B is the tread.

The vertical load on the front and rear axle wheels is as follows:

$$\begin{cases} F_{zf} = \dfrac{m\left(gb\cos\alpha - a_x h_g - g h_g \sin\alpha\right)}{l} \\ F_{zr} = \dfrac{m\left(ga\cos\alpha + a_x h_g + g h_g \sin\alpha\right)}{l} \end{cases} \tag{28}$$

Downloaded from SAE International by Georgia Institute of Technology, Sunday, April 06, 2025

where F_{zf} and F_{zr} represent the vertical loads on the front and rear axles, respectively, h_g denotes the height of center of mass, and α is the road slope.

The dynamic distribution based on the vertical loads of the front and rear axles should satisfy the following equation:

$$\begin{cases} \dfrac{T_{fl}+T_{fr}}{F_{zf}} = \dfrac{T_{rl}+T_{rr}}{F_{zr}} \\ \dfrac{T_{fr}-T_{fl}}{F_{zf}} = \dfrac{T_{rr}-T_{rl}}{F_{zr}} \end{cases} \tag{29}$$

By combining equations (27) to (29) and assuming the vehicle is on a level surface (α = 0), the distribution torque for each wheel is determined as follows:

$$\begin{cases} T_{fl} = \dfrac{gb - a_x h_g}{2gl}\left(T_d - \dfrac{2\Delta M r}{B}\right) \\ T_{fr} = \dfrac{gb - a_x h_g}{2gl}\left(T_d + \dfrac{2\Delta M r}{B}\right) \\ T_{rl} = \dfrac{ga + a_x h_g}{2gl}\left(T_d - \dfrac{2\Delta M r}{B}\right) \\ T_{rr} = \dfrac{ga + a_x h_g}{2gl}\left(T_d + \dfrac{2\Delta M r}{B}\right) \end{cases} \tag{30}$$

The distribution torque for each wheel is constrained by the road adhesion conditions, as shown in equation (31).

$$\left|T_{ij}\right| \le \min\left(T_{ij}, \mu r F_{zij}\right), ij \in \left\{fl,fr,rl,rr\right\} \tag{31}$$

where r is the wheel rolling radius, and μ is the road adhesion coefficient, F_{zij} represents the vertical load on each wheel.

Simulation Results and Analysis

To validate the effectiveness of the proposed distributed driving and braking ESC, a co-simulation with MATLAB/Simulink for control design and CarSim for vehicle modeling is developed. CarSim, a high-fidelity vehicle dynamics simulation tool, precisely simulates vehicle behavior in various driving conditions, ensuring reliable and accurate simulation results. The parameters of the DDEV in this study are shown in Table 2.

The proposed ESC is evaluated against a traditional single-wheel hydraulic differential braking ESC. The traditional ESC utilizes yaw rate as the control variable, with PID determining the additional yaw moment and distributing torque through hydraulic differential braking. Specifically, the PID determines the additional yaw moment based on yaw rate deviation. The driving state of the vehicle, characterized by the yaw rate deviation and the front wheel steering angle, determines the selection of the wheel for hydraulic braking to generate the required yaw moment. Consequently, the traditional ESC inevitably reduces speed during the control process, diminishing overall driving performance [21]. The braking pressure is calculated by equation (32), and the wheel selection rule for braking is presented in Table 3 [22].

TABLE 2 Parameters of the vehicle.

Parameter	Value
Vehicle mass m /kg	1300
Height of center of mass h_g /m	0.54
Wheelbase l /m	2.7
Distance from center of mass to front axle a/m	1.4
Wheel rolling radius r/m	0.31
Tread B/m	1.483
Cornering stiffness of front tire k_f/N·rad^{-1}	-92280
Cornering stiffness of rear tire k_r/N·rad^{-1}	-95699
Yaw moment of inertia I_z/kg·m^2	1343.1

TABLE 3 Differential braking wheel selection rule.

$\omega_r - \omega_{rd}$	δ_f	Driving state	Braking wheel
$\omega_r - \omega_{rd} > 0$	$\delta_f \ge 0$	Oversteer	Right front wheel
$\omega_r - \omega_{rd} < 0$	$\delta_f \le 0$	Oversteer	Left front wheel
$\omega_r - \omega_{rd} > 0$	$\delta_f \le 0$	Understeer	Right rear wheel
$\omega_r - \omega_{rd} < 0$	$\delta_f \ge 0$	Understeer	Left rear wheel
$\omega_r - \omega_{rd} = 0$	Arbitrary	Stability	\

$$P_{ij} = \frac{2\Delta M_t r}{BK_b}, ij \in \left\{fl,fr,rl,rr\right\} \tag{32}$$

where P_{ij} represents the braking hydraulic pressure, ΔM_t is the additional yaw moment from the traditional ESC, and K_b is the efficiency factor converting braking pressure into braking torque.

Validation of Vehicle State Estimation

To validate the effectiveness of the vehicle state estimator, a double lane change simulation is conducted at 80 km/h on a road with a 0.85 adhesion coefficient. The path for the double lane change is shown in Figure 5. The estimated states are compared with those obtained from CarSim. The results are presented in Figure 6.

As shown in Figures 6, the speed estimated by the PF basically matches the speed obtained from CarSim, with a maximum deviation of less than 0.45 km/h, satisfying the accuracy for speed estimation. Although a certain deviation in the estimated sideslip angle occurs around 5 seconds, the overall estimation error remains low throughout the maneuver, thus satisfying the requirements for stability control.

Downloaded from SAE International by Georgia Institute of Technology, Sunday, April 06, 2025

FIGURE 5 Path setup for double lane change maneuver.

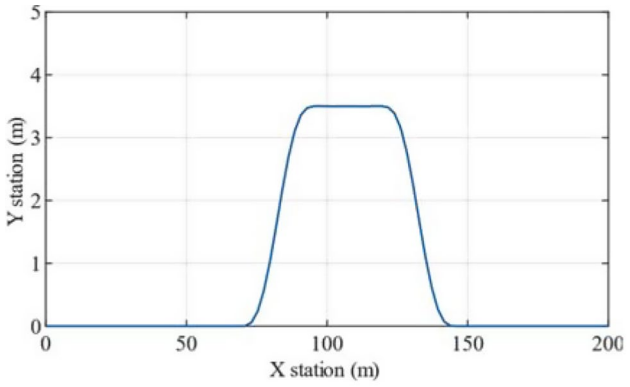

FIGURE 6 Estimation results of vehicle states: (a) sideslip angle; (b) speed.

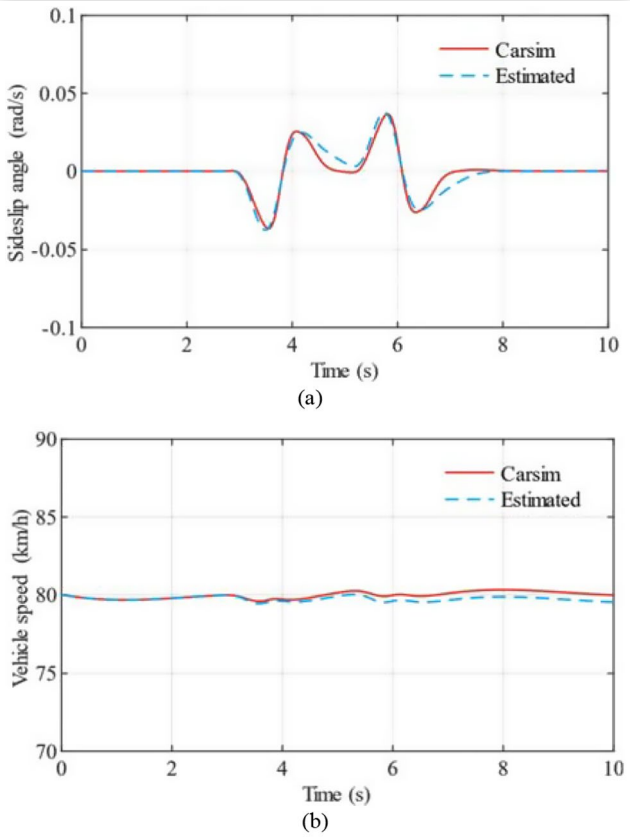

Comparison Validation of Stability Control

The stability control performance of the proposed distributed driving and braking ESC is validated through simulations of a double lane change maneuver on a joint road and a J-turn maneuver, compared to a traditional PID-based hydraulic differential braking ESC. In addition, the robustness of the proposed control method is analyzed.

Double Lane Change Maneuver A double lane change simulation is conducted on a joint road at a target speed of 55 km/h to evaluate the validity of the proposed ESC, particularly under varying road surface conditions. As shown in Figure 5, the road surface friction coefficient is set to 0.85 for the first 100 meters and then decreased to 0.4. The simulation results of the proposed ESC and the traditional ESC are shown in Figure 7.

As shown in Figures 7(a) and 7(e), the proposed ESC fully utilizes the independently controlled four-wheel system in DDEVs, generating additional yaw moment by driving the wheels on one side and applying regenerative braking to the opposite side. Furthermore, the proposed ESC fulfills the speed tracking requirements during the stability control process via a target speed tracking module, thereby enhancing the overall driving experience. In contrast, as shown in Figures 7(a) and 7(f), the traditional ESC generates additional yaw moment for stability through hydraulic differential braking on a single wheel. However, the application of hydraulic differential braking during stability control process inevitably causes a reduction in vehicle speed, thus failing to meet driving demands. Figure 7(b) demonstrates that the deviation between the actual and ideal yaw rates is significantly smaller with the proposed ESC. Even when road conditions abruptly change, the proposed ESC accurately tracks the ideal yaw rate, demonstrating superior performance. Figures 7(c) and 7(d) show that the proposed ESC effectively reduces the sideslip angle on the joint road, especially after approximately 7 seconds on the low-friction surface, with improved convergence and smaller deviations in the phase plane. This improvement is due to the adaptive adjustment of the sliding mode surface by the proposed FISMC, which achieves faster convergence on the low-friction surface, thereby enhancing adaptability under various driving conditions.

To further quantitatively and objectively evaluate the stability control performance of the proposed ESC and the traditional ESC, the root mean square error (RMSE) is introduced to represent the deviation between simulation results and reference values, as shown in the following equation:

$$RMSE = \sqrt{\frac{1}{N}\sum_{i=1}^{N}\left(y_i - r_i\right)^2} \tag{33}$$

where y_i represents the actual simulation results calculated by the proposed ESC and the traditional ESC, r_i denotes the reference values, and N is the total number of samples in the simulation process. The RMSE values for the two stability control strategies in double lane change maneuver are shown in Table 4. Since the RMSE values for vehicle speed, yaw rate, and sideslip angle in the proposed ESC are significantly lower than those in the traditional ESC, it can be concluded that the proposed ESC outperforms the traditional ESC in terms of stability control performance.

In conclusion, in the double lane change maneuver, the proposed ESC more accurately tracks desired values

Downloaded from SAE International by Georgia Institute of Technology, Sunday, April 06, 2025

FIGURE 7 Simulation results of distributed driving and braking ESC and traditional hydraulic differential braking ESC in double lane change maneuver: (a) vehicle speed; (b) yaw rate; (c) sideslip angle; (d) phase plane diagram; (e) motor torque for each wheel; (f) braking hydraulic pressure for each wheel.

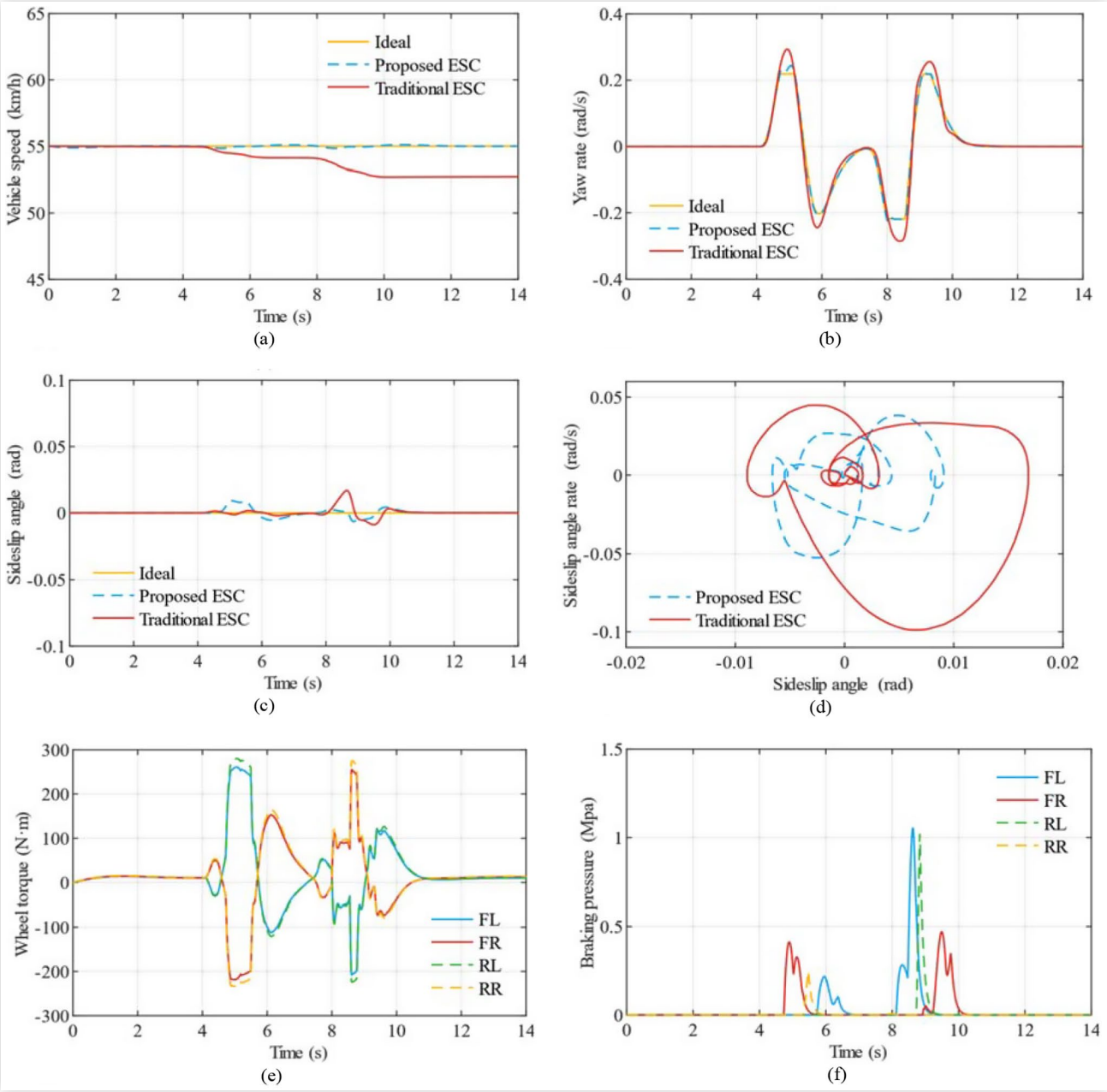

TABLE 4 RMSE results in double lane change maneuver.

RMSE	Proposed ESC	Traditional ESC
Vehicle speed	0.0697 km/h	1.4365 km/h
Yaw rate	0.0054 rad/s	0.0231 rad/s
Sideslip angle	0.0027 rad	0.0032 rad

and enhances stability while maintaining vehicle speed, compared to the traditional ESC.

J-Turn Maneuver Under a friction coefficient of 0.4 and a target speed of 80 km/h, the J-turn steering input is shown in Figure 8. The simulation results are presented in Figure 9.

Figures 9(a) and 9(e) show that the proposed ESC generates yaw moment by driving the wheels on one side and applying braking to the opposite side, maintaining stable vehicle speed using the target speed tracking module, and providing a better driving experience. In contrast, as shown in Figures 9(a) and 9(f), due to the implementation of single-wheel differential braking during stability control process, the traditional ESC results in speed loss and negatively impacts the driving experience. Figure 9(b) shows that the traditional ESC exhibits

Downloaded from SAE International by Georgia Institute of Technology, Sunday, April 06, 2025

FIGURE 8 Steering input for the j-turn maneuver.

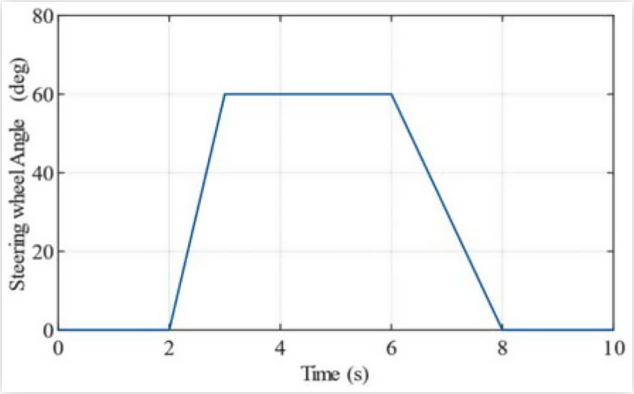

significant yaw rate overshoot throughout the J-turn maneuver, whereas the proposed ESC effectively tracks the desired yaw rate. Figures 9(c) and 9(d) further indicate that, compared to the traditional ESC, the proposed ESC substantially reduces the sideslip angle, with improved phase plane convergence and smoother trajectory evolution. This improvement is attributed to the adaptive adjustment of the sliding mode integral coefficient by the proposed FISMC, which responds to changes in the steering angle during sharp turns, thereby enhancing both the convergence speed of stability control.

Table 5 shows the RMSE values for the two stability strategies in the J-turn maneuver. The proposed ESC achieves significantly lower RMSE values for speed, yaw rate, and sideslip angle compared to the traditional ESC,

FIGURE 9 Simulation results of distributed driving and braking ESC and traditional hydraulic differential braking ESC in j-turn maneuver: (a) vehicle speed; (b) yaw rate; (c) sideslip angle; (d) phase plane diagram; (e) motor torque for each wheel; (f) braking hydraulic pressure for each wheel.

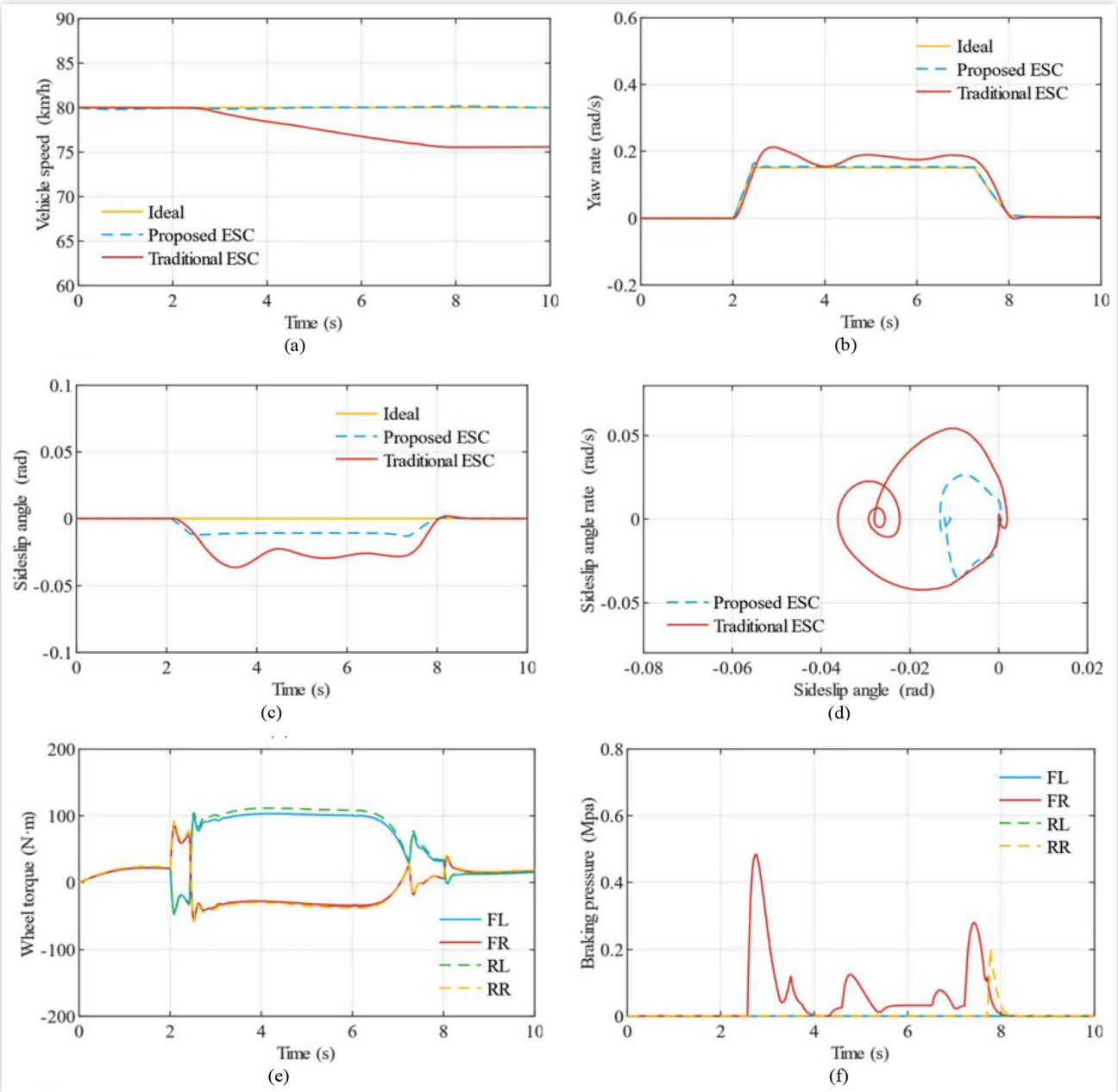

Downloaded from SAE International by Georgia Institute of Technology, Sunday, April 06, 2025

TABLE 5 RMSE results in J-turn maneuver.

RMSE	Proposed ESC	Traditional ESC
Vehicle speed	0.0957 km/h	2.9024 km/h
Yaw rate	0.0025 rad/s	0.0253 rad/s
Sideslip angle	0.0081 rad	0.0197 rad

especially with a 58.9% reduction in sideslip angle RMSE. This shows the proposed ESC ensures vehicle stability more efficiently under diverse driving conditions.

In conclusion, the proposed ESC demonstrates higher tracking precision, and improved lateral stability while maintaining vehicle speed stability, compared to the traditional ESC in the J-turn maneuver.

Robustness Analysis This study validates the robustness of the proposed ESC through simulations of the J-turn maneuver with different vehicle masses. Under a friction coefficient of 0.4 and a target speed of 80 km/h, the steering input for the J-turn maneuver is shown in Figure 8. The simulation results for the sideslip angle of the proposed ESC and traditional ESC are presented in Figure 10, where "M0" represents a vehicle mass of 1300 kg, and "M1" represents 1600 kg.

As shown in Figure 10, the proposed ESC effectively maintains a smaller sideslip angle despite changes in vehicle mass, whereas the traditional ESC exhibits a significant increase in sideslip angle with more pronounced fluctuations. The RMSE statistics of sideslip angle in Table 6 further substantiate the above analysis. These results demonstrate that the proposed ESC maintains effective stability control even with changes in vehicle model parameters, thereby fully validating the robustness of the proposed strategy.

FIGURE 10 Simulation results of the sideslip angle under J-turn maneuver with different vehicle masses.

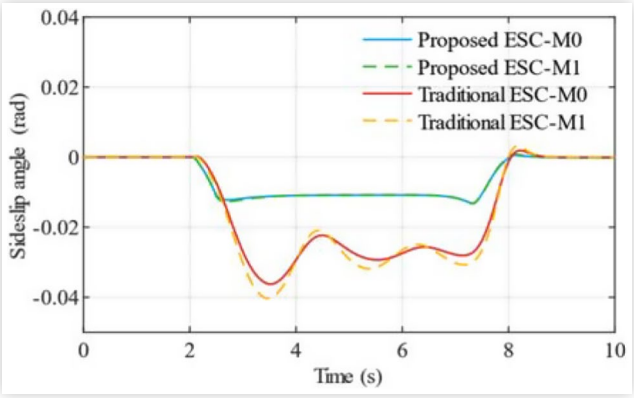

TABLE 6 RMSE of sideslip angle in J-turn maneuver.

RMSE (Sideslip angle)	Proposed ESC	Traditional ESC
M0 (1300 kg)	0.0081 rad	0.0197 rad
M1 (1600 kg)	0.0082 rad	0.0209 rad

Summary

To enhance the stability of DDEVs under various driving conditions, this paper proposes a hierarchical control strategy for distributed driving and braking ESC based on PF and FISMC. The strategy consists of three layers: vehicle state estimation, target torque decision, and dynamic torque distribution. First, The vehicle state estimation layer uses a 3DOF vehicle model and the PF algorithm to estimate real-time vehicle states such as sideslip angle and vehicle speed. Next, The target torque decision layer comprises a target speed tracking controller and a yaw moment decision controller, which utilizes the FISMC algorithm to determine additional yaw moment by comparing estimated and ideal yaw rates and sideslip angles, and dynamically adjusts the sliding mode surface based on vehicle state and driving conditions. Finally, the dynamic torque distribution layer allocates driving and regenerative braking torque to each wheel based on changes in tire vertical load.

A co-simulation platform using MATLAB/Simulink and CarSim validated the proposed control strategy under double lane change and J-turn maneuvers. Results show that the state estimator accurately estimates vehicle states such as sideslip angle and vehicle speed. Compared to the traditional hydraulic differential braking ESC, the proposed strategy more effectively maintains vehicle speed and adapts to changing driving conditions, thereby improving the lateral stability of DDEVs.

References

1. Guo, K. and Ding, H., "The Effect of Differential Braking on the Lateral Torque of Automobiles at the Tire Adhesion Limit," *Automobile Engineering* 02 (2002): 101-104.
2. Abbasi, N., Dehghani, M., Asemani, M.H., and Abolpour, R., "Robust Observer Design for LPV Systems Using Kronecker Sum and Direct Searching," *Isa Transactions* 136 (2023): 210-222.
3. Zhou, X., Shen, H., Wang, Z., and Wang, J., "Self-Scheduled L 1 Robust Vehicular Sideslip Angle Estimation," in *presented at 2022 American Control Conference (ACC)*, USA, June 8-10, 2022.
4. Tian, M., Zhang, Q., Tian, D., Jin, L. et al., "Pre-Stability Control for in-Wheel-Motor-Driven Electric Vehicles with Dynamic State Prediction," *IEEE Transactions on Intelligent Vehicles* 9, no. 3 (2024): 4541-4554.
5. Wang, H., Xu, S., Zhou, D., Wang, X. et al., "Vehicle Center of Gravity Side Slip Angle Estimation Based on Fuzzy Sliding Mode Observer and Sensor Signal Integral Fusion," *Journal of Beijing Institute of Technology* 42, no. 07 (2022): 713-722.
6. Wang, P., Fan, X., Chen, X., Yi, J. et al., "UKF Estimation Method of Centroid Slip Angle for Vehicle Stability Control," *International Journal of Control, Automation and Systems* 21, no. 7 (2023): 2259-2266.

Downloaded from SAE International by Georgia Institute of Technology, Sunday, April 06, 2025

7. Lin, F., Zhao, N., and Xu, S., "Automotive State Estimation Technology Based on Particle Filter Algorithm," *Journal of Agricultural Machinery* 42, no. 02 (2011): 23-27+22.
8. Fu, Y., Xie, R., Kaku, C., and Zheng, H., "Coordinated Control of Trajectory Tracking and Yaw Stability of a Hub-Motor-Driven Vehicle Based on Four-Wheel-Steering," SAE Technical Paper 2024-01-2767 (2024), https://doi.org/10.4271/2024-01-2767.
9. Lath, U., Kakkar, S., Agarwal, A., Ashok, B. et al., "Modelling and Validation of a Control Algorithm for yaw Stability & Body Slip Control Using PID & Fuzzy Logic Based Controllers," SAE Technical Paper 2019-28-0054 (2019), https://doi.org/10.4271/2019-28-0054.
10. Wang, H., Wu, J., Chen, Z., He, R. et al., "Vehicle Yaw Stability Model Predictive Control Strategy for Dynamic and Multi-Objective Requirements," SAE Technical Paper 2024-01-2324 (2024), https://doi.org/10.4271/2024-01-2324.
11. Jonasson, M., Andreasson, J., Solyom, S., Jacobson, B. et al., "Utilization of Actuators to Improve Vehicle Stability at the Limit: From Hydraulic Brakes toward Electric Propulsion," *Journal of Dynamic Systems, Measurement, and Control* 133, no. 5 (2011).
12. Song, Y., Shu, H., Chen, X., and Luo, S., "Direct-Yaw-Moment Control of Four-Wheel-Drive Electrical Vehicle Based on Lateral Tyre-Road Forces and Sideslip Angle Observer," *IET Intelligent Transport Systems* 13, no. 2 (2019): 356-366.
13. Fu, C., Hoseinnezhad, R., Bab-Hadiashar, A., and Jazar, R.N., "Direct Yaw Moment Control for Electric and Hybrid Vehicles with Independent Motors," *International Journal of Vehicle Design* 69, no. 1-4 (2015): 1-24.
14. Yu, Z., *Automobile Theory, Sixth Edition* (Machinery Industry Press, 2018)
15. Chen, C., Zheng, H., and Zong, C., "Personalized Design of Variable Transmission Ratio and Selection Switching Strategies Considering Drivers' Steering Characteristics," *SAE Int. J. Veh. Dyn., Stab., and NVH* 8, no. 4 (2024), https://doi.org/10.4271/10-08-04-0028.
16. Li, Y., Hu, Y., and Zou, T., "Yaw Stability Control of Electric Vehicles Driven by Hub Motors," *Journal of Chongqing University* 40, no. 12 (2017): 24-34.
17. Wang, Z., Chen, C., Jiang, Q., Zheng, H. et al., "State Estimation of Drive-by-Wire Chassis Vehicle Based on Dual Unscented Particle Filter Algorithm," *Chinese Journal of Mechanical Engineering* 37, no. 1 (2024): 11.
18. Huang, X.P., *Principles and Applications of Particle Filtering: Matlab Simulation* (Electronic Industry Press, 2017)
19. Alipour, H., Bannae Sharifian, M.B., and Sabahi, M., "A Modified Integral Sliding Mode Control to Lateral Stabilisation of 4-Wheel Independent Drive Electric Vehicles," *Vehicle System Dynamics* 52, no. 12 (2014): 1584-1606.
20. Zhai, L., Sun, T., and Wang, J., "Electronic Stability Control Based on Motor Driving and Braking Torque Distribution for a Four in-Wheel Motor Drive Electric Vehicle," *IEEE Transactions on Vehicular Technology* 65, no. 6 (2016): 4726-4739.
21. Yu, Z. and Feng, Y., "Overview of the Development of Dynamic Control for Distributed Drive Electric Vehicles," *Journal of Mechanical Engineering* 49, no. 08 (2013): 105-114.
22. Zhang, J., Jiang, H., Li, L., Liu, Q. et al., "Hierarchical Vehicle Stability Control Strategy Based on Unscented Kalman Filter Estimation," SAE Technical Paper 2022-01-0294 (2022), https://doi.org/10.4271/2022-01-0294.

Contact Information

Hongyu Zheng
Professor
National Key Laboratory of Automotive Chassis Integration and Bionics, Jilin University, China
zhenghy@jlu.edu.cn or zhy_jlu@163.com

Acknowledgments

This research was funded by FAW Volkswagen China Environmental Protection Foundation Automotive Environmental Protection Innovation Leadership Program.

© 2025 SAE International. All rights reserved. No part of this publication may be reproduced, stored in a retrieval system, transmitted, in any form or by any means, electronic, mechanical, photocopying, recording, or otherwise, or used for text and data mining, AI training, or similar technologies, without the prior written permission of SAE.

Positions and opinions advanced in this work are those of the author(s) and not necessarily those of SAE International. Responsibility for the content of the work lies solely with the author(s).

ISSN 0148-7191